UC Irvine

UC Irvine Electronic Theses and Dissertations

Title

Biomedical Simulator Using Nonlinear Finite Element Modeling of the Human Head

Permalink

https://escholarship.org/uc/item/9c7571cf

Author

Ma, Shiting

Publication Date

2018

Peer reviewed|Thesis/dissertation

eScholarship.org Powered by the California Digital Library
University of California

UNIVERSITY OF CALIFORNIA,
IRVINE

Biomedical Simulator Using Nonlinear Finite Element Modeling of the Human Head

THESIS

submitted in partial satisfaction of the requirements
for the degree of

MASTER OF SCIENCE

in Biomedical Engineering

by

Shiting Ma

Thesis Committee:
Professor Frithjof Kruggel, Chair
Professor Zoran Nenadic
Assistant Professor Michelle Digman

2018

© 2018 Shiting Ma

Table of Contents

List of Figures

List of Tables

Acknowledgements

My deepest gratitude goes first to Professor Kruggel, my supervisor, for his great patience and effort to guide me throughout this whole project. His advice and encouragement is very important to me during the past two years. I would also like to express my appreciation to my thesis committee members: Professor Nenadic and Professor Digman for their helpful suggestions. Without their help this thesis could not be finished.

Lastly, my thanks would go to my family, without their support, I would never have a chance to start an academic career in U.S.

Abstract of the Thesis

Biomedical Simulator Using Nonlinear FEM Modeling of Human Head

By

Shiting Ma

Master of Science in Biomedical Engineering

University of California, Irvine, 2018

Professor Frithjof Kruggel, Chair

Biomaterials, including brain tissue, usually have nonlinear material properties. In this project, a human head simulator using the finite element method (FEM) was improved by adding an implementation of a nonlinear material model into it. The Ogden model is chosen to be implemented in this project because of its good accuracy to model the brain tissue. This work aims at improving the validity of impact simulation tests. Results show that the nonlinear model was successfully implemented into the simulator and a difference was discovered when conducting impact simulation. In the simulation using a nonlinear model, the deformation of brain tissue is larger than the deformation using a linear model.

1 Introduction

1.1 Motivation

Severe traumatic brain injury often causes death or permanent disability, especially in children and infants [1]. The most common causes of traumatic brain injury include violence, transportation accidents, construction accidents and sports [2]. Although trauma can be caused by a large acceleration or deceleration, most of traumatic brain injuries are caused by an impact [3].

Considerable effort has been spent developing treatments and therapies to save patients' life as well as to help them recover from injury. Imaging methods such as computational cranial tomography (CCT) and magnetic resonance imaging (MRI) have been developed to estimate the consequence of a trauma [4]. However, what exactly happens when an impact is applied to the head and how the brain is injured from the impact is less known. In fact, understanding how and where the external mechanical forces cause the internal brain trauma would also be helpful for early diagnosis and for making a good treatment decision.

This project focuses on the development of a biomechanical simulator for modeling the consequences of an external impact on the human head. Specifically, this simulation system is based on a finite element analysis with the data coming from an anatomical MRI scan [5]. The aim of this thesis is to extend material properties to model nonlinear material behavior and provide more realistic solutions.

1.2 Biomaterial Mechanical Properties

Biomaterials, such as bone, muscle, skin, soft tissue and fluid inside our body, often have very complex mechanical characteristics.

Biomaterials are often composite and contain substructures with very different material properties. As a result, the complexity of the components of material leads to difficulty in predicting their mechanical behavior [6]. Because of the complex inner structure, biomaterial show different behavior with respect to the spatial directions; for example, white matter inside the brain usually consists of bundles of neural axons, which likely exhibit anisotropic properties [7].

In order to estimate the interaction between a biomaterial and an external force, proper simplification and approximation are necessary. Specific kinds of biomaterials are usually modeled as elastomers [8].

An elastomer is a body with elasticity. Elasticity is usually described with the relationship between stress (the force applied per unit area) and corresponding strain (the amount that the material deforms per unit length). Elasticity can be separated into two main categories: linear elasticity and nonlinear elasticity. Linear means that the ratio of stress and strain remains constant when deformation occurs to the material, for example, a metal spring. On the other hand, nonlinear elasticity means that the relationship between stress and strain is not constant, as for a rubber band [9]. Fig 1.1 shows the linear and nonlinear stress-strain relationship.

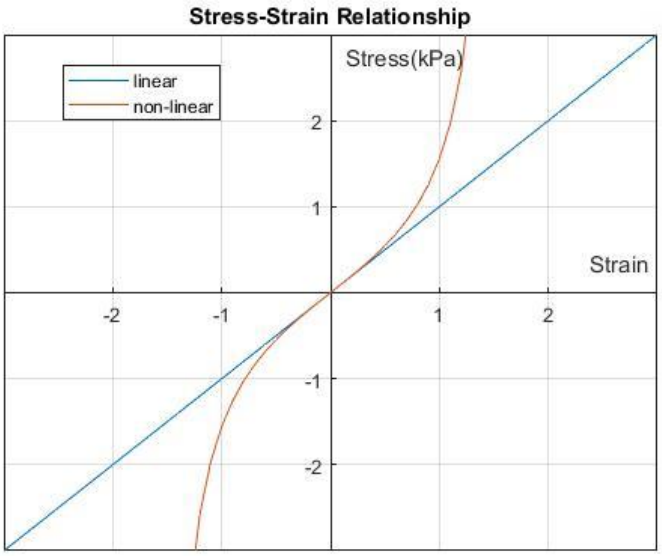

Fig. 1.1 Linear and nonlinear stress-strain relationship

Material properties of brain tissues, including white matter and grey matter, can only be considered as linear when the displacement is not too large. In contrast, the skull or muscles, brain tissue is relatively soft and can easily experience large deformation with only small mechanical force [10]. As shown in Fig. 1.1, with a large deformation, the difference between linear and nonlinear model cannot be ignored. Thus, brain tissue should be represented with nonlinear properties in a bionumerical simulation [8].

A method of testing brain tissue material property is presented in [11]. Researchers harvested specimens from different locations of the brain and apply a uniaxial tension-compression on the specimens. The tension and compression are applied to the specimen in a cyclic way, and the speed is slow enough so that the influence of the velocity and the acceleration can be ignored. This testing is called uniaxial quasi-static cyclic tension-compression test. Fig. 1.2 shows the setup of the in vitro experiment setup and Fig. 1.3 shows the anatomical location of the harvested specimen..

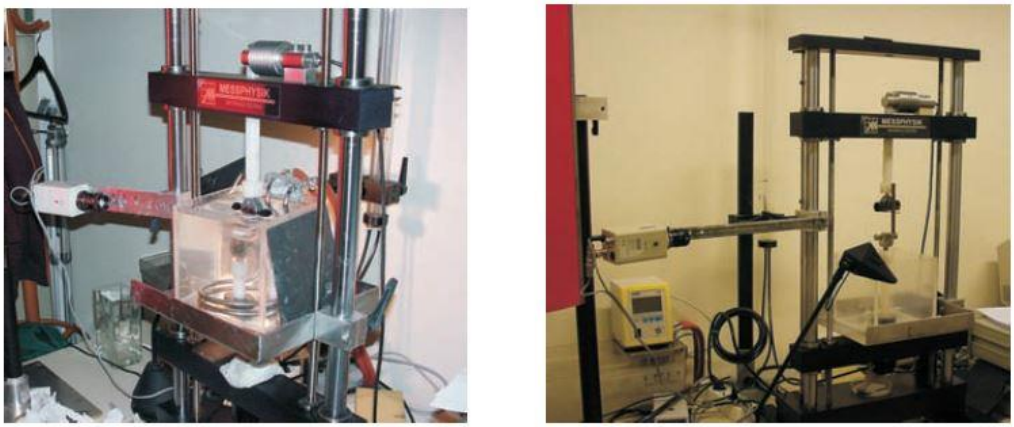

Fig. 1.2 Experimental setup, from[11]

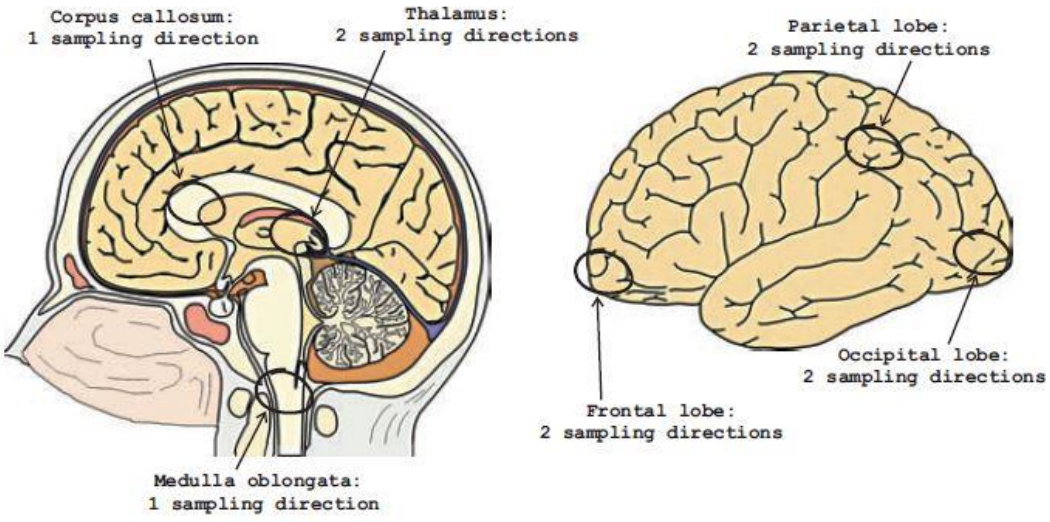

Fig. 1.3 Sample harvest location, from [11]

The nonlinear stress-strain relationship shown in Fig. 1.1 can be represented by different parametric models. We choose to use the Ogden model [12] as a material model to be implemented in our simulation system. One reason for this is based on the literature that has reported a good fit with experimental results in [11]. This general model can easily be modified into other kinds of elastic models such as the Neo-Hookean model, the Mooney-Rivlin model or the Yeoh Model by a parameter transformation [13].

1.3 Finite Element Model

The finite element method is a numerical method for solving boundary value problems for partial differential equations (PDE). A large number of engineering and physical problems are described by PDEs. However, few systems described by PDEs have an analytical solution, thus, various kinds of numerical methods have been developed to provide a numerical solution of PDEs. The finite element method is one of the most effective and widely used approaches [14].

In mechanical engineering, FEM is usually used to design new products and conduct simulations to visualize in-structural mechanical quantities such as stress and displacement. Simulations using FEM greatly help industries to optimize the time and raw-material costs during the manufacturing process, as well as ensure the quality of the products [15].

By discretization of a continuous body into finite elements and considering elements as homogeneous, the problem of solving partial differential equation can be transformed into the problem of solving a set of linear equations, which can be implemented in software [16]. Large problems, such as modeling impacts on highly resolved head models, require super-computers for an efficient solution.

In this project, FEM is chosen to simulate the impact consequence on the human head due to the need to visualize a possible cause of intracranial damage, such as large deformation of elements or a large pressure change in the brain tissue during and after the impact.

This method allows conducting mechanical analyses on objects with complex structures. After dividing the object into small elements, every element can have different and independent material properties. This is helpful to model the complex micro structure of the human brain. In the human head, brain tissues are known to have nonlinear elasticities. Applying a nonlinear model to brain tissue, simulation results are expected to be closer to reality than only modeling the brain tissue as linear elastomers [12]. However, other tissues such as the skull are much stiffer and can be approximated by linear elasticity models. These two kinds of elasticity models are able to work simultaneously in one simulation system by using FEM.

Since it is not ethic to conduct controlled scientific impact tests on human head, and the results from the feasible animal experiments are difficult to extrapolate to humans because of the difference in head and brain geometry, the prediction of brain damage after an impact produced by a simulator is necessary.

The aim of this project is to introduce the modeling of nonlinear material properties into an existing software for the simulation of impact on the human head. As mentioned before, brain tissue has nonlinear material properties. In order to get the accurate position and severity of the possible intracranial damage from the simulation, the implementation of nonlinear model into the simulator is necessary.

2 Methods

2.1 Linear Elasticity Derivation

First, it is necessary to have a review of the mathematical derivation of the linear material model in order to introduce some basic definition and theory. The following derivation is based on [13].

2.1.1 Definition of Stress and Strain

Stress is defined as force per unit area in uniaxial state and one dimensional structure. However, in three-dimensional situation, a thorough understanding and a clear notation of stress is necessary.

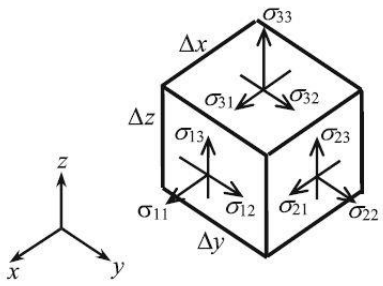

Fig. 2.1 Stress inside object, from [13]

In Fig. 2.1, the components of the stress on the three Cartesian planes can be described using a virtual cube. In fact, this cube has no extent because it is not a physical cube. The stress at a point inside a solid structure can be defined as a tensor of rank 2:

$$\left[\sigma_{ij}\right]=\begin{bmatrix}\sigma_{11} & \sigma_{12} & \sigma_{13}\\ \sigma_{21} & \sigma_{22} & \sigma_{23}\\ \sigma_{31} & \sigma_{32} & \sigma_{33}\end{bmatrix} \tag{1}$$

As the moment in z-axis must be equal to zero when the body is under static equilibrium, σ_{21} and σ_{12} should be equal to each other, the same as x-axis and y-axis. As a result,

$$\sigma_{12} = \sigma_{21},\ \sigma_{13} = \sigma_{31},\ \sigma_{23} = \sigma_{32} \tag{2}$$

So the stress tensor can also be represented as

$$\left[\sigma_{ij}\right] = \begin{bmatrix} \sigma_{11} & \sigma_{12} & \sigma_{13} \\ \sigma_{12} & \sigma_{22} & \sigma_{23} \\ \sigma_{13} & \sigma_{23} & \sigma_{33} \end{bmatrix} \tag{3}$$

As is seen above, there are only six independent elements in the matrix, so the stress tensor can be written as a pseudo-vector

$$\left\{\boldsymbol{\sigma}\right\} = \begin{Bmatrix} \sigma_{11} \\ \sigma_{22} \\ \sigma_{33} \\ \sigma_{12} \\ \sigma_{23} \\ \sigma_{13} \end{Bmatrix} \tag{4}$$

Strain is defined as the change of length per unit original length in one dimensional situation, but it can also be generalized to describe the solid deformation in three-dimensional situation.

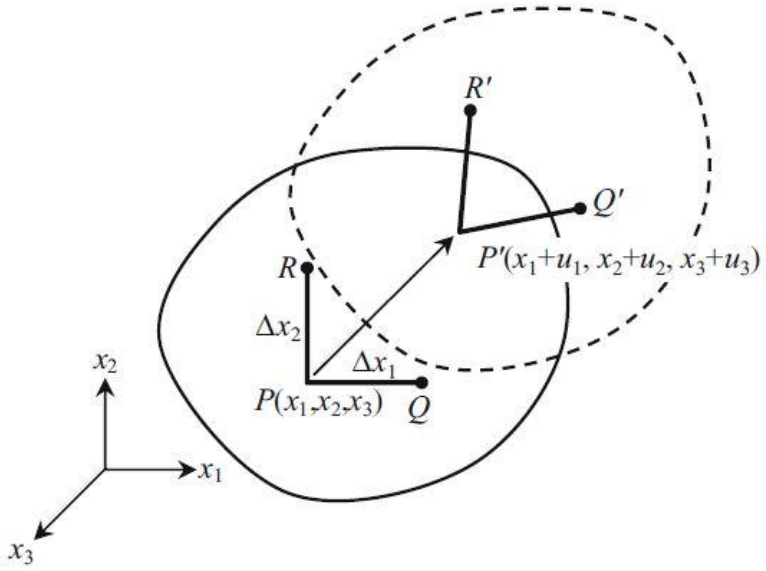

Fig. 2.2 Deformation of line segment, from [13]

As shown in Fig. 2.2, points P, Q and R are in the undeformed body and are moved to P', Q' and R' in the deformed body. The displacement of point P is represented as u_1, u_2 and u_3 in the direction of x_1, x_2 and x_3, respectively.

The nominal strain is defined as

$$\varepsilon_{11} = \frac{P'Q' - PQ}{PQ} = \frac{\partial u_1}{\partial x_1} \tag{5}$$

Similarly, we can define nominal strains in other directions as

$$\varepsilon_{22} = \frac{\partial u_2}{\partial x_2}, \varepsilon_{33} = \frac{\partial u_3}{\partial x_3} \tag{6}$$

From Fig. 2.2, the angle between P'Q' and PQ can be derived as

$$\theta_1 = \frac{x_2^{Q'} - x_2^{Q}}{\Delta x_1} = \frac{\partial u_2}{\partial x_1} \tag{7}$$

The angle between P'R' and PR can be similarly derived as

$$\theta_2 = \frac{x_2^{R'} - x_2^{R}}{\Delta x_2} = \frac{\partial u_1}{\partial x_2} \tag{8}$$

The definition of the shear strain in x_1x_2 plane is

$$\gamma_{12} = \theta_1 + \theta_2 = \frac{\partial u_1}{\partial x_2} + \frac{\partial u_2}{\partial x_1} \tag{9}$$

The shear strains in x_2x_3 and x_1x_3 plane are similarly defined as

$$\gamma_{23} = \frac{\partial u_2}{\partial x_3} + \frac{\partial u_3}{\partial x_2}, \gamma_{13} = \frac{\partial u_1}{\partial x_3} + \frac{\partial u_3}{\partial x_1} \tag{10}$$

Since it is obvious that $\gamma_{12} = \gamma_{21}$, we define the tensorial shear strain element as

$$\{\boldsymbol{\varepsilon}\} = \begin{Bmatrix} \varepsilon_{11} \\ \varepsilon_{22} \\ \varepsilon_{33} \\ \gamma_{12} \\ \gamma_{23} \\ \gamma_{13} \end{Bmatrix} = \begin{Bmatrix} \varepsilon_{11} \\ \varepsilon_{22} \\ \varepsilon_{33} \\ 2\varepsilon_{12} \\ 2\varepsilon_{23} \\ 2\varepsilon_{13} \end{Bmatrix} \tag{11}$$

or in tensor form

$$\left[\varepsilon_{ij}\right]=\begin{bmatrix}\varepsilon_{11} & \varepsilon_{12} & \varepsilon_{13}\\ \varepsilon_{12} & \varepsilon_{22} & \varepsilon_{23}\\ \varepsilon_{13} & \varepsilon_{23} & \varepsilon_{33}\end{bmatrix}$$

(12)

Since both stress and strain are rank-2 tensors, the relationship between them need a rank-4 tensor to describe. For a linear elastic material, the relationship between stress and strain can be written as

$$\boldsymbol{\sigma}=\mathbf{D}:\boldsymbol{\varepsilon}$$

(13)

where the symbol ":" is the contraction operator, which means

$$\sigma_{ij}=\sum_{k=1}^{3}\sum_{l=1}^{3}D_{ijkl}\varepsilon_{kl}$$

(14)

Here **D** is called the elasticity tensor. In linear case, **D** is independent of geometry of the object. Since tensor **D** is symmetric, the relationship between stress and strain can also be written in matrix-vector form

$$\{\boldsymbol{\sigma}\}=[\mathbf{D}]\cdot\{\boldsymbol{\varepsilon}\}$$

(15)

where [**D**] is a 6 by 6 symmetric matrix. Here the symbol "{}" is used to represent vectors and "[]" for matrix. If the material is considered isotropic, [**D**] is characterized by two material constants, Young's modulus E and the Poisson ratio ν as follows:

$$[\mathbf{D}] = \frac{E}{(1+\nu)(1-2\nu)} = \begin{bmatrix} 1-\nu & \nu & \nu & 0 & 0 & 0 \\ \nu & 1-\nu & \nu & 0 & 0 & 0 \\ \nu & \nu & 1-\nu & 0 & 0 & 0 \\ 0 & 0 & 0 & \frac{1}{2}-\nu & 0 & 0 \\ 0 & 0 & 0 & 0 & \frac{1}{2}-\nu & 0 \\ 0 & 0 & 0 & 0 & 0 & \frac{1}{2}-\nu \end{bmatrix} \tag{16}$$

2.2 Nonlinear Elasticity Derivation

2.2.1 Stress and Strain Measures in Large Deformation

When the deformation is large enough, the difference between undeformed and deformed geometries is noticeable. Thus, it is important to understand how to represent a large deformation of a material and how to define stress and strain in such case.

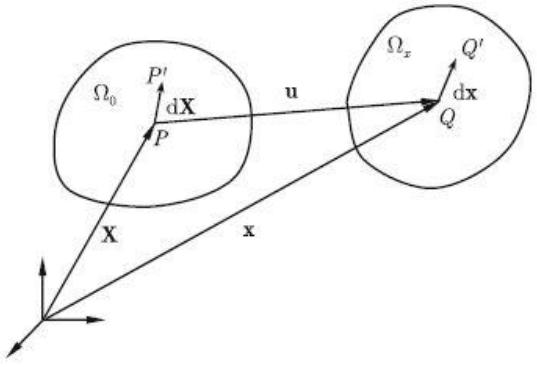

Fig. 2.3 Undeformed and deformed geometries, From [13]

As is shown in Fig. 2.3, point P is identified by vector $\mathbf{X} = [X_1, X_2, X_3]$ in undeformed geometry and is mapped to point Q in deformed geometry, which is identified by vector $\mathbf{x} = [x_1, x_2, x_3]$.

Vector **u** is the displacement of point P. Also, the vector d**X** deformed to d**x**. The relationship between d**X** and d**x** can be expressed as follows:

$$d\mathbf{x} = \frac{\partial \mathbf{x}}{\partial \mathbf{X}} d\mathbf{X} \tag{17}$$

Here the deformation gradient tensor **F** is defined as

$$\mathbf{F} = \frac{\partial \mathbf{x}}{\partial \mathbf{X}} = \mathbf{1} + \nabla_0 \mathbf{u} \tag{18}$$

which is also written as

$$\mathbf{F} = \begin{Bmatrix} 1+\frac{\partial u_1}{\partial x_1} & \frac{\partial u_1}{\partial x_2} & \frac{\partial u_1}{\partial x_3} \\ \frac{\partial u_2}{\partial x_1} & 1+\frac{\partial u_2}{\partial x_2} & \frac{\partial u_2}{\partial x_3} \\ \frac{\partial u_3}{\partial x_1} & \frac{\partial u_3}{\partial x_2} & 1+\frac{\partial u_3}{\partial x_3} \end{Bmatrix} \tag{19}$$

The Lagrangian strain uses the undeformed geometry as a reference. Consider the two differential elements, d**X** and d**x**. The vector d**X** is deformed to d**x**. The change in squares of length of these two vectors can be expressed as follows:

$$\begin{aligned} \|d\mathbf{x}\|^2 - \|d\mathbf{X}\|^2 &= d\mathbf{x}^T d\mathbf{x} - d\mathbf{X}^T d\mathbf{X} \\ &= d\mathbf{X}^T \mathbf{F}^T \mathbf{F} d\mathbf{X} - d\mathbf{X}^T d\mathbf{X} \\ &= d\mathbf{X}^T \left(\mathbf{F}^T \mathbf{F} - \mathbf{1} \right) d\mathbf{X} \end{aligned} \tag{20}$$

In Eq. (20), $\mathbf{F}^T\mathbf{F}$ is an important quantity and is defined as a right Cauchy-Green deformation tensor:

$$\mathbf{C} = \mathbf{F}^T\mathbf{F}$$

(21)

The Lagrangian strain is defined as

$$\mathbf{E} = \frac{1}{2}(\mathbf{C} - \mathbf{1})$$

(22)

In terms of displacement gradient, the Lagrangian stain is also written as

$$\mathbf{E} = \frac{1}{2}(\frac{\partial \mathbf{u}}{\partial \mathbf{X}} + \frac{\partial \mathbf{u}^T}{\partial \mathbf{X}} + \frac{\partial \mathbf{u}^T}{\partial \mathbf{X}}\frac{\partial \mathbf{u}}{\partial \mathbf{X}}) = \frac{1}{2}(\nabla_0\mathbf{u} + \nabla_0\mathbf{u}^T + \nabla_0\mathbf{u}^T\nabla_0\mathbf{u})$$

(23)

When the displacement is small, the Lagrangian strain is approximated by the infinitesimal strain tensor:

$$\boldsymbol{\varepsilon} = \frac{1}{2}(\nabla_0\mathbf{u} + \nabla_0\mathbf{u}^T)$$

(24)

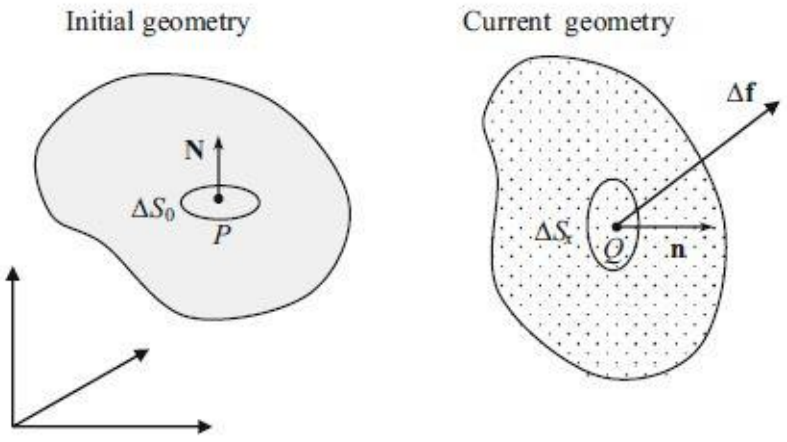

Fig. 2.4 Stress vectors in undeformed and deformed geometries, from [13]

Similar to strain, stress also depends on the frame of reference. As shown in Fig. 2.4, the stress vector at point Q in deformed geometry can be written as

$$\mathbf{t} = \lim_{\Delta S_x \to 0} \frac{\Delta \mathbf{f}}{\Delta S_x} = \boldsymbol{\sigma}\mathbf{n}$$

(25)

where ΔS_x is the area of differential element, $\Delta \mathbf{f}$ is the force acting on it and $\mathbf{n}$ is the unit normal of the area. Here $\boldsymbol{\sigma}$ is called Cauchy stress.

A different stress tensor is defined using the undeformed geometry as reference:

$$\mathbf{T} = \lim_{\Delta S_0 \to 0} \frac{\Delta \mathbf{f}}{\Delta S_0} = \mathbf{P}^T \mathbf{N}$$

(26)

where $\mathbf{P}$ is known as the first Piola-Kirchhoff stress tensor. Since $\mathbf{P}$ is not symmetric, the second Piola-Kirchhoff stress is defined as

$$\mathbf{S} = \mathbf{P}\mathbf{F}^{-T} = J\mathbf{F}^{-1}\boldsymbol{\sigma}\mathbf{F}^{-T}$$

(27)

where J is the determinant of the deformation gradient.

2.2.2 Nonlinear Elastic Analysis

The stress-strain relation describes the behavior of a material between deformation and internal force caused by deformation.

In an elastic material, the strain energy density W is defined as following:

$$W(\mathbf{E}) = \frac{1}{2}\mathbf{E} : \mathbf{D} : \mathbf{E}$$

(28)

where **D** is the rank-4 elasticity tensor. In contrast to the linear model, here **D** is not a constant under deformation. As a result, the relationship between second Piola-Kirchhoff stress and Lagrangian strain is obtained as following:

$$\mathbf{S} \equiv \frac{\partial W(\mathbf{E})}{\partial \mathbf{E}} = \mathbf{D} : \mathbf{E} \tag{29}$$

Also, we can obtain:

$$\mathbf{D} = \frac{\partial \mathbf{S}}{\partial \mathbf{E}} = 4\frac{\partial^2 W}{\partial \mathbf{C}^2} \tag{30}$$

To simplify the notation in the following derivation, we define notations of several tensor operators. In following definition, **a** and **b** are rank-1 tensors, while **A** and **B** are rank-2 tensors.

$(\mathbf{a} \otimes \mathbf{b})_{ij} = \mathbf{a}_i \mathbf{b}_j$,

$(\mathbf{A} \otimes \mathbf{B})_{ijkl} = \mathbf{A}_{ij} \mathbf{B}_{kl}$,

$(\mathbf{A} \underline{\otimes} \mathbf{B})_{ijkl} = \mathbf{A}_{ik} \mathbf{B}_{jl}$, $(\mathbf{A} \overline{\otimes} \mathbf{B})_{ijkl} = \mathbf{A}_{il} \mathbf{B}_{jk}$,

$(\mathbf{A} \underline{\overline{\otimes}} \mathbf{B})_{ijkl} = \frac{1}{2}\left((\mathbf{A} \underline{\otimes} \mathbf{B}) + (\mathbf{A} \overline{\otimes} \mathbf{B})\right)$

As is mentioned before, **C** is the right Cauchy-Green deformation tensor. We define the invariants of **C** as

$$I_1 = tr(\mathbf{C}),\ \ I_2 = \frac{1}{2}\left[(tr(\mathbf{C}))^2 - tr(\mathbf{C}^2)\right],\ \ I_3 = \det \mathbf{C} \tag{31}$$

λ_a (a=1,2,3) are the eigenvalues of **C**, and the eigenvalue-bases $\mathbf{M}_a$ (a=1,2,3) are related to the eigenvectors $\mathbf{n}_a$ of **C** by:

$$\mathbf{M}_a = \mathbf{n}_a \otimes \mathbf{n}_a$$

(32)

Here we use a hyperelastic model, more specifically, the Ogden model to simulate the brain tissue because of its good accuracy when the tissue is under large deformation. The following derivation is from [17].

The Ogden constitutive law is widely used to model rubber-like materials. The strain energy density function is given as follows

$$W = \sum_{i=1}^{N} \frac{\mu_i}{\alpha_i}\left(\lambda_1^{\alpha_i/2} + \lambda_2^{\alpha_i/2} + \lambda_3^{\alpha_i/2} - 3\right) + \sum_{i=1}^{N} \frac{\mu_i}{\alpha_i \beta_i}\left(I_3^{-\alpha_i \beta_i/2} - 1\right)$$

(33)

where N, μ_i, α_i and β_i are material parameters. Note the $\lambda_a, (a = 1,2,3)$ is the eigenvalues of the Cauchy-Green deformation tensor **C**.

For convenience of the following derivation, we define

$$\begin{aligned} W &= \sum_{i=1}^{3} W_1^i + W_2^i, \\ W_1^i &= \lambda_1^{\alpha_i/2} + \lambda_2^{\alpha_i/2} + \lambda_3^{\alpha_i/2}, \\ W_2^i &= I_3^{-\alpha_i \beta_i/2} \end{aligned}$$

(34)

Make a new notation that $\alpha = \alpha_i / 2$ and $\beta = -\alpha_i \beta_i / 2$. The Eq. (35) becomes

$$\begin{aligned} W_1 &= \lambda_1^{\alpha} + \lambda_2^{\alpha} + \lambda_3^{\alpha}, \\ W_2 &= I_3^{\beta} \end{aligned}$$

(35)

The stress tensor is calculated as following:

$$\mathbf{S}=\sum_{a=1}^{3}S\left(\lambda_a\right)\mathbf{M}_a-\left(\sum_{i=1}^{N}\mu_i I_3^{-\alpha_i\beta_i/2}\right)\mathbf{C}^{-1} \tag{36}$$

where $S\left(\lambda_a\right)$ is defined by

$$S\left(\lambda_a\right)=\sum_{i=1}^{N}\mu_i\lambda_a^{\alpha_i/2-1} \tag{37}$$

As mentioned in Eq. (30) elasticity tensor **D** is calculated as

$$\mathbf{D}=\frac{\partial\mathbf{S}}{\partial\mathbf{E}}=4\frac{\partial^2 W}{\partial\mathbf{C}^2}=4\left(\sum_{i=1}^{N}\frac{\mu_i}{\alpha_i}\frac{\partial^2 W_1^i}{\partial\mathbf{C}^2}+\sum_{i=1}^{N}\frac{\mu_i}{\alpha_i\beta_i}\frac{\partial^2 W_2^i}{\partial\mathbf{C}^2}\right) \tag{38}$$

By deriving twice Eq. (35), we can obtain

$$\begin{aligned}\mathbf{D}&=4\sum_{i=1}^{N}\left(\frac{\mu_i}{\alpha_i}\frac{\partial^2 W_1^i}{\partial\mathbf{C}^2}+\frac{\mu_i}{\alpha_i\beta_i}\frac{\partial^2 W_2^i}{\partial\mathbf{C}^2}\right)\\&=2\sum_{i=1}^{N}\mu_i\cdot\left\{\begin{array}{l}\left\{\left(\alpha-1\right)\sum_{a=1}^{3}\lambda_a^{\alpha-2}\mathbf{M}_a\otimes\mathbf{M}_a+\sum_{a=1}^{3}\frac{\lambda_a^{\alpha-1}-\lambda_b^{\alpha-1}}{\lambda_a-\lambda_b}\left[\mathbf{M}_a\underline{\overline{\otimes}}\mathbf{M}_b+\mathbf{M}_b\underline{\overline{\otimes}}\mathbf{M}_a\right]\right\}\\+I_3^{\beta}\left\{\beta\mathbf{C}^{-1}\otimes\mathbf{C}^{-1}-\mathbf{C}^{-1}\underline{\overline{\otimes}}\mathbf{C}^{-1}\right\}\end{array}\right\}\end{aligned} \tag{39}$$

where N, μ_i, α_i and β_i are material parameters, α and β are defined as $\alpha=\alpha_i/2$ and $\beta=-\alpha_i\beta_i/2$. When $\lambda_i\to\lambda_j$,

$$\lim_{\lambda_i\to\lambda_j}\left(\frac{\lambda_i^{\alpha-1}-\lambda_j^{\alpha-1}}{\lambda_i-\lambda_j}\right)=\left(\alpha-1\right)\lambda_i^{\alpha-2} \tag{40}$$

2.3 Finite Element Model

This section introduces the mathematical background underlying finite element models in biomechanics. The following derivation is based on [13].

2.3.1 Static Finite Element Equation

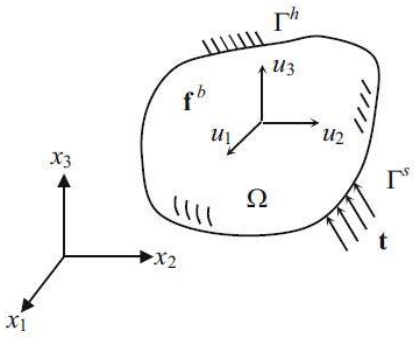

Fig. 2.5 Deformable body under equilibrium, from [13]

A body shown in Fig. 2.5 is under static equilibrium under the applied body force $\mathbf{f}^b$ and the surface traction $\mathbf{t}^{(n)}$. The domain inside the body is Ω and the boundary is Γ. The surface traction is applied on Γ^s.

Since the body is under static equilibrium, it follows the principle of minimum potential energy and the variational equation is established as following

$$\int_\Omega \boldsymbol{\varepsilon}\left(\bar{\mathbf{u}}\right) : \mathbf{D} : \boldsymbol{\varepsilon}\left(\mathbf{u}\right) d\Omega - \int_\Omega \bar{\mathbf{u}} \cdot \mathbf{f}^b d\Omega - \int_{\Gamma^s} \bar{\mathbf{u}} \cdot \mathbf{t} d\Gamma = 0 \tag{41}$$

where $\bar{\mathbf{u}}$ is the virtual displacement.

The variational equation (Eq.(41)) mentioned above generally does not have an analytical solution. In the context of finite element modeling the body is discretize the body into a set of finite elements, and within each finite element, the result is approximated in a simple polynomial form.

Consider the isoparametric 3-dimensional hexahedral element with eight nodes shown in Fig. 2.6

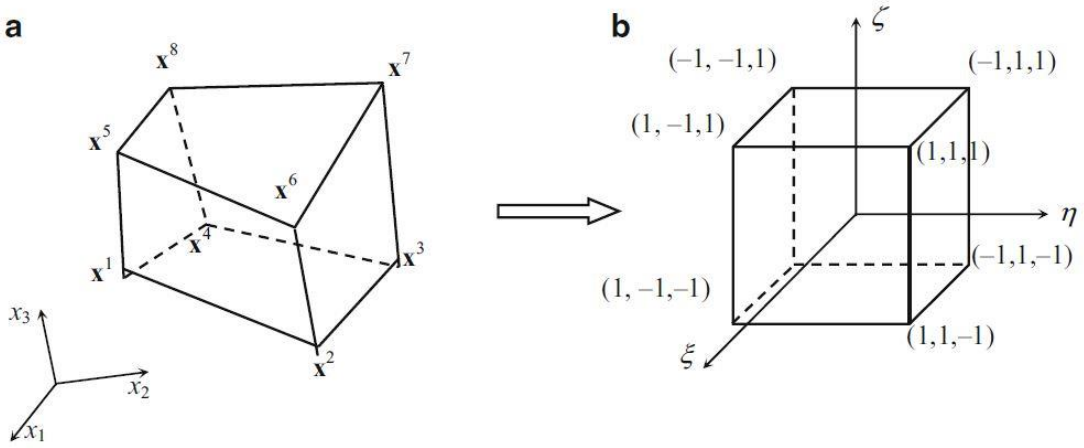

Fig. 2.6 3D isotropic hexahedron element, from [13]

Fig. 2.6a shows a deformed element and 2.6b shows a reference coordinate of the element. Let $\mathbf{u}_I = [u_{I1}, u_{I2}, u_{I3}]$ be the displacement at node I and $\boldsymbol{\xi}_I = [\xi_I, \eta_I, \zeta_I]$ be the corresponding reference coordinate. The coordinate and displacement of the element is defined as

$$\mathbf{x}(\boldsymbol{\xi}) = \sum_{I=1}^{8} N_I(\boldsymbol{\xi})\mathbf{x}_I \tag{42}$$

and

$$\mathbf{u}(\boldsymbol{\xi}) = \sum_{I=1}^{8} N_I(\boldsymbol{\xi})\mathbf{u}_I \tag{43}$$

where $\mathbf{x}_I$ is the coordinate at node I and $N_I(\boldsymbol{\xi})$ is the interpolation function at node I.

Then the relationship between displacement and strain is established as

$$\boldsymbol{\varepsilon}(\mathbf{u}) = \sum_{I=1}^{8} \mathbf{B}_I \mathbf{u}_I \tag{44}$$

where

$$\mathbf{B}_I = \begin{Bmatrix} N_{I,1} & 0 & 0 \\ 0 & N_{I,2} & 0 \\ 0 & 0 & N_{I,3} \\ N_{I,2} & N_{I,1} & 0 \\ 0 & N_{I,3} & N_{I,2} \\ N_{I,3} & 0 & N_{I,1} \end{Bmatrix} \tag{45}$$

and

$$N_{I,1} = \frac{\partial N_I}{\partial x_1}, N_{I,2} = \frac{\partial N_I}{\partial x_2}, N_{I,3} = \frac{\partial N_I}{\partial x_3} \tag{46}$$

Here we define **B** as the strain-displacement matrix

$$\mathbf{B} = \begin{bmatrix} \mathbf{B}_1 & \mathbf{B}_2 & \mathbf{B}_3 & \ldots & \mathbf{B}_8 \end{bmatrix}. \tag{47}$$

Here for the convenience of expression, we also define the interpolation matrix **N** as

$$\mathbf{N}_I = \begin{bmatrix} N_I & 0 & 0 \\ 0 & N_I & 0 \\ 0 & 0 & N_I \end{bmatrix}, \mathbf{N} = \begin{bmatrix} \mathbf{N}_1 & \mathbf{N}_2 & \mathbf{N}_3 & \ldots & \mathbf{N}_8 \end{bmatrix} \tag{48}$$

Rewrite the variational equation inside one element as the following

$$\bar{\mathbf{u}} \int_{\Omega} \mathbf{B}^T \mathbf{D}\mathbf{B} d\Omega \, \mathbf{u} - \sum_{I=1}^{8} \bar{\mathbf{u}}_I \int_{\Omega} N_I(\xi) \cdot \mathbf{f}_b d\Omega - \sum_{I=1}^{8} \bar{\mathbf{u}}_I \int_{\Gamma^s} N_I(\xi) \cdot \mathbf{t} d\Gamma = 0 \tag{49}$$

The nodal displacement is defined as

$$\mathbf{d} = [u_{11}, u_{12}, u_{13}, u_{21}, u_{22}, u_{23}, ..., u_{81}, u_{82}, u_{83}]^T \tag{50}$$

where u_{Ii} is the displacement on node I in direction i. $\bar{\mathbf{d}}$ is the rank-1 tensor of nodal virtual displacements, and **k** is the 24 by 24 element stiffness matrix for a single hexahedral element, the equation is written as

$$\bar{\mathbf{d}}^T \mathbf{k}\mathbf{d} = \bar{\mathbf{d}}^T \mathbf{f}_{ele} \tag{51}$$

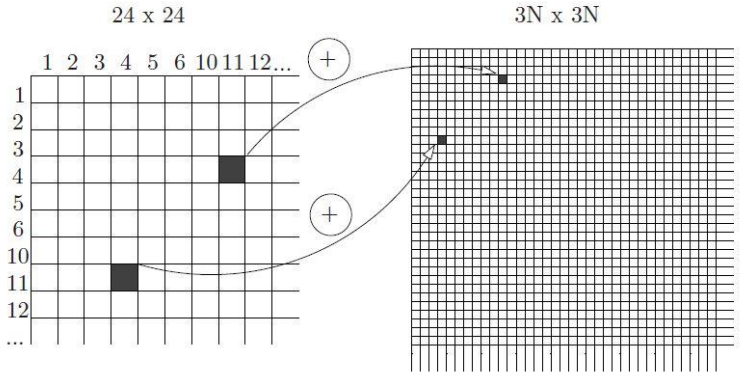

Fig. 2.7 Assembling the global matrices, from[18]

Here we need to assemble the element vectors and matrices together into the global vectors and matrices. For example, element stiffness matrix **k** is a 24 by 24 matrix, then the global stiffness matrix is a 3N by 3N matrix, N is the total node number of the whole object. As shown in Fig.2.7,

the entries of element matrices (left) are added to the corresponding entries of the global matrix (right).

After summing up every elemental equation together and considering the concentrated load **L** the global equation is written as

$$\mathbf{Ku} = \mathbf{r} \tag{52}$$

where

$$\begin{aligned}
&\mathbf{r} = \mathbf{F}_b + \mathbf{F}_T + \mathbf{L} \\
&\mathbf{F}_b = \sum_m \sum_{I=1}^{8} \bar{\mathbf{u}}_I \int_\Omega N_I(\xi) \cdot \mathbf{f}_b d\Omega = \sum_m \int_\Omega \mathbf{N} \cdot \mathbf{f}_b d\Omega \\
&\mathbf{F}_T = \sum_m \sum_{I=1}^{8} \bar{\mathbf{u}}_I \int_{\Gamma^s} N_I(\xi) \cdot \mathbf{t} d\Gamma = \sum_m \int_{\Gamma^s} \mathbf{N} \cdot \mathbf{t} d\Gamma
\end{aligned} \tag{53}$$

The global nodal displacement **u** can be solved with given applied load, fixed nodes and global stiffness matrix **K**. Here, the static linear finite element equation had been established, and the partial differential equation problem is converted into linear equation problem.

2.3.2 Dynamic Finite Element Equation

For an object with mass m with an applied force r(t) and the displacement u(t), it obeys following relationship

$$F_i + F_d + F_s = r(t) \tag{54}$$

where F_i is the inertial force, F_d is the damping force and F_s is the restoring force.

Note that the inertial force F_i is calculated with the mass m and the acceleration $\ddot{u}(t)$ as $F_i = m\ddot{u}(t)$ according to Newton's law.

With linear elasticity, the restoring force F_s and the damping force F_d are considered as proportional to the deformation $u(t)$ and velocity $\dot{u}(t)$ so it is also written as following:

$$m\ddot{u}(t) + c\dot{u}(t) + ku(t) = r(t) \tag{55}$$

where c is the damping coefficient and k is stiffness.

After discretization mentioned above, the equation becomes

$$\mathbf{M}\ddot{\mathbf{u}}(t) + \mathbf{G}\dot{\mathbf{u}}(t) + \mathbf{K}\mathbf{u}(t) = \mathbf{r}(t) \tag{56}$$

Eq. (56) is called as a dynamic finite element equation, where **M** is called mass matrix, **G** is called damping matrix and **K** is stiffness matrix mentioned previously. Here, with mass density ρ, **M** is written as

$$\mathbf{M} = \sum_m \int_\Omega \rho \mathbf{N}^T \mathbf{N} d\Omega \tag{57}$$

The damping matrix **G** is the linear combination of M and K:

$$\mathbf{G} = \alpha_d \mathbf{M} + \beta_d \mathbf{K} \tag{58}$$

where α_d and β_d are damping coefficients.

2.3.3 Newmark's Method

To solve a dynamic finite element model, various of methods have been developed. Here, Newmark's method is chosen because of its numerical stability. It is described in this section based on [16].

The first step of solution is the descretize time into small time intervals Δt and define Newmark parameters α_N and β_N. Then, define the initial displacement, velocity and acceleration as $\mathbf{u}_0$, $\dot{\mathbf{u}}_0$, $\ddot{\mathbf{u}}_0$. In the Newmark integration scheme, following assumptions are used:

$$\begin{aligned}\dot{\mathbf{u}}_{t+\Delta t} &= \dot{\mathbf{u}}_t + \left[(1-\beta_N)\ddot{\mathbf{u}}_t + \beta_N \ddot{\mathbf{u}}_{t+\Delta t}\right]\Delta t \\ \mathbf{u}_{t+\Delta t} &= \mathbf{u}_t + \dot{\mathbf{u}}_t \Delta t + \left[(0.5-\alpha_N)\ddot{\mathbf{u}}_t + \alpha_N \ddot{\mathbf{u}}_{t+\Delta t}\right]\Delta t^2\end{aligned} \tag{59}$$

where α_N and β_N are parameters to be chosen to obtain integration accuracy and stability. Here we choose to use unconditionally stable scheme (setting $\alpha_N = \frac{1}{4}$ and $\beta_N = \frac{1}{2}$).

After this, calculate the integration constants $a_0, a_1, a_2 \cdots a_7$ with α_N, β_N and Δt :

$$\begin{aligned}a_0 &= \frac{1}{\alpha_N \Delta t^2}; a_1 = \frac{\beta_N}{\alpha_N \Delta t}; a_2 = \frac{1}{\alpha_N \Delta t}; a_3 = \frac{1}{2\alpha_N} - 1 \\ a_4 &= \frac{\beta_N}{\alpha_N} - 1; a_5 = \frac{\Delta t}{2}\left(\frac{\beta_N}{\alpha_N} - 2\right); a_6 = \Delta t(1-\beta_N); a_6 = \beta_N \Delta t\end{aligned} \tag{60}$$

and form up the modified stiffness matrix as follows:

$$\hat{\mathbf{K}} = \mathbf{K} + a_0 \mathbf{M} + a_1 \mathbf{G} \tag{61}$$

The Newmark integration process is conducted as following procedure at every time step:

1. Calculate the effective loads:

$$\mathbf{R}_{t+\Delta t} = \mathbf{R}_{t+\Delta t} + \mathbf{M}\left(a_0\mathbf{u}_t + a_2\dot{\mathbf{u}}_t + a_3\ddot{\mathbf{u}}_t\right) + \mathbf{G}\left(a_1\mathbf{u}_t + a_4\dot{\mathbf{u}}_t + a_5\ddot{\mathbf{u}}_t\right) \tag{62}$$

2. Solve for displacement **u**:

$$\hat{\mathbf{K}}\mathbf{u}_{t+\Delta t} = \mathbf{R}_{t+\Delta t} \tag{63}$$

3. Calculate acceleration and velocity at $t+\Delta t$:

$$\begin{aligned}\ddot{\mathbf{u}}_{t+\Delta t} &= a_0\left(\mathbf{u}_{t+\Delta t} - \mathbf{u}_t\right) - a_2\dot{\mathbf{u}}_t - a_3\ddot{\mathbf{u}}_t \\ \dot{\mathbf{u}}_{t+\Delta t} &= \dot{\mathbf{u}}_t + a_6\ddot{\mathbf{u}}_t + a_7\ddot{\mathbf{u}}_{t+\Delta t}\end{aligned} \tag{64}$$

After going through all the time steps the finite element equation is solved at every time point.

If Newmark's method is used to solve a nonlinear dynamic problem, the stiffness matrix **K** is replaced by tangent stiffness matrix $\mathbf{K}_T$ and displacement **u** by an increment displacement $\Delta\mathbf{u}$.

2.4 Nonlinear Finite Element Model Implementation

In previous section, the FEM formulation of the linear elastic model has been described. We will now extend dynamic analysis to include elements with nonlinear material properties, such as discussed in Section 2.2. The following derivation is based on [13].

2.4.1 Solution Procedures for Nonlinear Equations

Before introducing the nonlinear FEM equation, we need to have a glance at the typical solution procedures of nonlinear equation first.

Consider the following system of nonlinear equations:

$$\mathbf{P(u) = f} \tag{65}$$

where $\mathbf{u} = \{u_1, u_2, \ldots u_n\}^T$ is a vector of unknowns, $\mathbf{f} = \{f_1, f_2, \ldots, f_n\}^T$ is a vector of known quantities, and $\mathbf{P}(\mathbf{u}) = \{P_1(\mathbf{u}), P_2(\mathbf{u}), \ldots, P_n(\mathbf{u})\}$ represents vector of nonlinear functions of $\mathbf{u}$, which is different from the linear model, $\mathbf{P}(\mathbf{u}) = \mathbf{Ku}$.

Since $\mathbf{P}(\mathbf{u})$ is a nonlinear function of $\mathbf{u}$, the nonlinear analysis focused on how to solve Eq.(65) accurately. Here an iteration method is needed. Starting from $\mathbf{u}^0$, the increment of the solution $\Delta\mathbf{u}$ is obtained by solving a system of linear equations. The solution is iteratively updated by the increment until a specific convergence criteria is satisfied.

This iterative method called Newton-Raphson method is popular in numerical analysis to find the roots of nonlinear equations.

The Newton-Raphson method assumes an initial estimate, $\mathbf{u}^0$, and find its increment, $\Delta\mathbf{u}$, with the derivative at the initial estimation point, so that the new estimate, $\mathbf{u}^0 + \Delta\mathbf{u}$, is close to the solution.

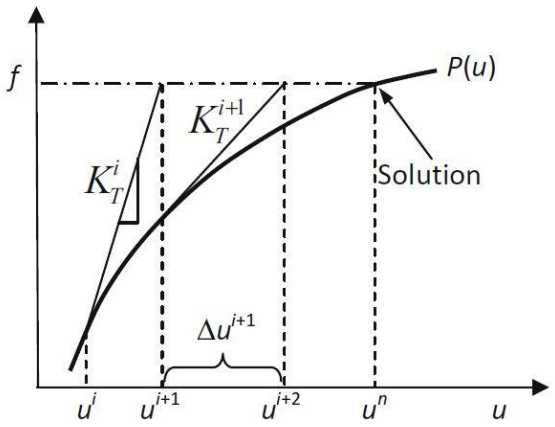

Fig. 2.8 Newton-Raphson method for nonlinear equation P(u) = f, From [13]

As shown in Fig. 2.8, in order to find the increment, the nonlinear equations are locally approximated by linear ones. Suppose a solution at the *i* th iteration is known and is designated by $\mathbf{u}^i$. The solution at the next iteration can be approximated as following:

$$\mathbf{P}(\mathbf{u}^{i+1}) \approx \mathbf{P}(\mathbf{u}^i) + \mathbf{K}_T^i(\mathbf{u}^i) \cdot \Delta\mathbf{u}^i = \mathbf{f} \tag{66}$$

where $\mathbf{K}_T^i(\mathbf{u}^i)$ is the Jacobian matrix at ith iteration and $\Delta\mathbf{u}^i$ is the solution increment. The goal is to calculate $\Delta\mathbf{u}^i$ and iteratively update solution $\mathbf{u}^{i+1}$.

After rearranging Eq. (66), the linearized equation is written as

$$\mathbf{K}_T^i \cdot \Delta\mathbf{u}^i = \mathbf{f} - \mathbf{P}(\mathbf{u}^i) \tag{67}$$

Here $\mathbf{K}_T^i$ is a function of $\mathbf{u}^i$. After the displacement increment is solved, the new approximation is obtained as follows:

$$\mathbf{u}^{i+1} = \mathbf{u}^i + \Delta\mathbf{u}^i \tag{68}$$

And the unbalanced force (residual force) is defined as follow:

$$\mathbf{r}^{i+1} = \mathbf{f} - \mathbf{P}(\mathbf{u}^{i+1})$$

(69)

When specific convergence criteria are satisfied, the solution is considered as the accurate solution and the process stops.

2.4.2 Nonlinear Finite Element Equation

The nonlinear variational equation is established as

$$\int_{0\Omega} \frac{\partial W(\mathbf{E})}{\partial \mathbf{E}} : \bar{\mathbf{E}} d\Omega - \int_{0\Omega} \bar{\mathbf{u}}^T \mathbf{f}^b d\Omega - \int_{0\Gamma^s} \bar{\mathbf{u}}^T \mathbf{t} d\Gamma = 0$$

(70)

Here **S** is the second Piola-Kirchhoff stress and **E** is the Lagrangian Strain as mentioned before.

From Section 2.4.1, we established that the solution of this equation requires linearization.

The linearization of the energy form in Eq. (73) can be written as

$$L\left[\int_{0\Omega} \mathbf{S} : \bar{\mathbf{E}} d\Omega\right] = \int_{0\Omega} \left[\Delta\mathbf{S} : \bar{\mathbf{E}} + \mathbf{S} : \Delta\bar{\mathbf{E}}\right] d\Omega = \int_{0\Omega} \left[\bar{\mathbf{E}} : \mathbf{D} : \Delta\mathbf{E} + \mathbf{S} : \Delta\bar{\mathbf{E}}\right] d\Omega$$

(71)

The descretized variation of Lagrangian strain $\bar{\mathbf{E}}$ can be written as

$$\bar{\mathbf{E}} = \mathbf{B}_N \bar{\mathbf{d}}$$

(72)

where $\bar{\mathbf{d}}$ is the variation of nodal displacements and $\mathbf{B}_N$ is the nonlinear displacement-strain matrix defined as

$$\mathbf{B}_N = \begin{Bmatrix} F_{11}N_{1,1} & F_{21}N_{1,1} & F_{31}N_{1,1} & \cdots & F_{11}N_{n,1} & F_{21}N_{n,1} & F_{31}N_{n,1} \\ F_{12}N_{1,2} & F_{22}N_{1,2} & F_{32}N_{1,2} & \cdots & F_{12}N_{n,2} & F_{22}N_{n,2} & F_{32}N_{n,2} \\ F_{13}N_{1,3} & F_{23}N_{1,3} & F_{33}N_{1,3} & \cdots & F_{13}N_{n,3} & F_{23}N_{n,3} & F_{33}N_{n,3} \\ F_{11}N_{1,2} & F_{21}N_{1,1} & 0 & \cdots & F_{11}N_{n,2} & F_{21}N_{n,1} & 0 \\ 0 & F_{22}N_{1,3} & F_{32}N_{1,2} & \cdots & 0 & F_{22}N_{n,3} & F_{32}N_{n,2} \\ F_{13}N_{1,3} & 0 & F_{33}N_{1,1} & \cdots & F_{13}N_{n,3} & 0 & F_{33}N_{n,1} \end{Bmatrix}$$

(73)

where F is the deformation tensor defined in Eq.(19)

The discrete energy form can be derived as

$$\int_{{}^0\Omega} \mathbf{S} : \bar{\mathbf{E}} d\Omega \;=\; \bar{\mathbf{d}}^T \int_{{}^0\Omega} \mathbf{B}_N{}^T \mathbf{S} d\Omega \;\equiv\; \bar{\mathbf{d}}^T \mathbf{f}^{\text{int}}$$

(74)

Note that from this equation the internal force at every element is calculated as

$$\mathbf{f}^{\text{int}} = \int_{{}^0\Omega} \mathbf{B}_N{}^T \mathbf{S} d\Omega$$

(75)

The discrete load form can be derived as

$$\iint_{{}^0\Omega} \bar{\mathbf{u}}^T \mathbf{f}^b d\Omega + \int_{{}^0\Gamma^s} \bar{\mathbf{u}}^T \mathbf{t} d\Gamma \;=\; \sum_{I=1}^{N_e} \bar{\mathbf{u}}_I^T \left\{ \iint_{{}^0\Omega} N_I(\boldsymbol{\xi}) \mathbf{f}^b d\Omega + \int_{{}^0\Gamma^s} N_I(\boldsymbol{\xi}) \mathbf{t} d\Gamma \right\} \;\equiv\; \bar{\mathbf{d}}^T \mathbf{f}^{ext}$$

(76)

The discrete version of variational equation can be established as following:

$$\bar{\mathbf{d}}^T \mathbf{f}^{\text{int}}(\mathbf{d}) = \bar{\mathbf{d}}^T \mathbf{f}^{ext}$$

(77)

Consider the equation based on incremental nodal displacement as following:

$$\bar{\mathbf{d}}^T \mathbf{k}_T \Delta\mathbf{d} = \bar{\mathbf{d}}^T \left\{ \mathbf{f}^{ext} - \mathbf{f}^{\text{int}} \right\}$$

(78)

The tangent stiffness matrix at element is calculated as

$$\mathbf{k}_T = \int_{0\Omega} \left[\mathbf{B}_N{}^T \mathbf{D} \mathbf{B}_N + \mathbf{B}_G{}^T \Sigma \mathbf{B}_G \right] d\Omega$$

(79)

where $\boldsymbol{\Sigma}$ is defined as

$$\boldsymbol{\Sigma} = \begin{bmatrix} S_{11} & S_{12} & S_{13} & 0 & 0 & 0 & 0 & 0 & 0 \\ S_{12} & S_{22} & S_{23} & 0 & 0 & 0 & 0 & 0 & 0 \\ S_{13} & S_{23} & S_{33} & 0 & 0 & 0 & 0 & 0 & 0 \\ 0 & 0 & 0 & S_{11} & S_{12} & S_{13} & 0 & 0 & 0 \\ 0 & 0 & 0 & S_{12} & S_{22} & S_{23} & 0 & 0 & 0 \\ 0 & 0 & 0 & S_{13} & S_{23} & S_{33} & 0 & 0 & 0 \\ 0 & 0 & 0 & 0 & 0 & 0 & S_{11} & S_{12} & S_{13} \\ 0 & 0 & 0 & 0 & 0 & 0 & S_{12} & S_{22} & S_{23} \\ 0 & 0 & 0 & 0 & 0 & 0 & S_{13} & S_{23} & S_{33} \end{bmatrix}$$

(80)

and $\mathbf{B_G}$ is defined as

$$\mathbf{B_G} = \begin{bmatrix} N_{1,1} & 0 & 0 & \cdots & N_{n,1} & 0 & 0 \\ N_{1,2} & 0 & 0 & \cdots & N_{n,2} & 0 & 0 \\ N_{1,3} & 0 & 0 & \cdots & N_{n,3} & 0 & 0 \\ 0 & N_{1,1} & 0 & \cdots & 0 & N_{n,1} & 0 \\ 0 & N_{1,2} & 0 & \cdots & 0 & N_{n,2} & 0 \\ 0 & N_{1,3} & 0 & \cdots & 0 & N_{n,3} & 0 \\ 0 & 0 & N_{1,1} & \cdots & 0 & 0 & N_{n,1} \\ 0 & 0 & N_{1,2} & \cdots & 0 & 0 & N_{n,2} \\ 0 & 0 & N_{1,3} & \cdots & 0 & 0 & N_{n,3} \end{bmatrix}$$

(81)

After summing up over every element, the global tangent stiffness matrix $\mathbf{K}_T$ and the internal force $\mathbf{f}$ is calculated as

$$\mathbf{K}_T = \sum_m \int_{0\Omega} \left[\mathbf{B}_N{}^T \mathbf{D} \mathbf{B}_N + \mathbf{B}_G{}^T \Sigma \mathbf{B}_G \right] d\Omega$$
$$\mathbf{f} = \sum_m \mathbf{f}^{\text{int}}$$

(82)

During every step inside the Newton Ralphson iteration, Newmark's method brings in the relationship between displacement, velocity and acceleration. Establishing the equation system with the mass matrix **M**, damping matrix **G**, internal force vector **f** and tangent stiffness matrix $\mathbf{K}_T$, an increment of displacement at every time step is obtained. This process is iterated throughout all time steps of the simulation.

3 Experiments and Results

3.1 Homogeneous Deformation of Rubber Model

The first experiment reproduces the three homogeneous deformation examples listed in [17] in order to confirm the correct implementation of the nonlinear finite element method.

In this experiment a rubber cube (single element model) that obeys a three term Ogden model (N=3) is used for testing purpose. The material parameters are:

$\mu_1 = 0.66$, $\mu_2 = 0.0012$, $\mu_3 = -0.01$,

$\alpha_1 = 1.3$, $\alpha_2 = 5$, $\alpha_3 = -2$,

$\beta_1 = 10$, $\beta_2 = 10$, $\beta_3 = 10$.

The following several different cases are considered:

Case 1: See Fig. 3.1(a). Only F_x is applied on the cube and the cube is undergoing a uniaxial stretch.

In this case, an analytical solution is given in [12] as following:

$$F_x = A_0 \sum_{i=1}^{N} \left(\lambda_x^{\alpha_i - 1} - \lambda_x^{-\alpha_i/2 - 1} \right) \tag{84}$$

The result is shown in Fig. 3.2. The numerical result calculated by finite element method has a good match with the analytical curve.

Case 2: See Fig. 3.1(b). F_x and F_z are applied on the cube such that $u_z=0$.

The simulation result is shown in Fig. 3.3. The result is as same as the result presented in [17].

Case 3: See Fig. 3.1(c). F_x, F_y and F_z are applied on the cube such that $u_x=u_y=u_z$. So the cube is under hydrostatic pressure. The result is shown in Fig. 3.4 This simulation also successfully reproduced the results presented in [17].

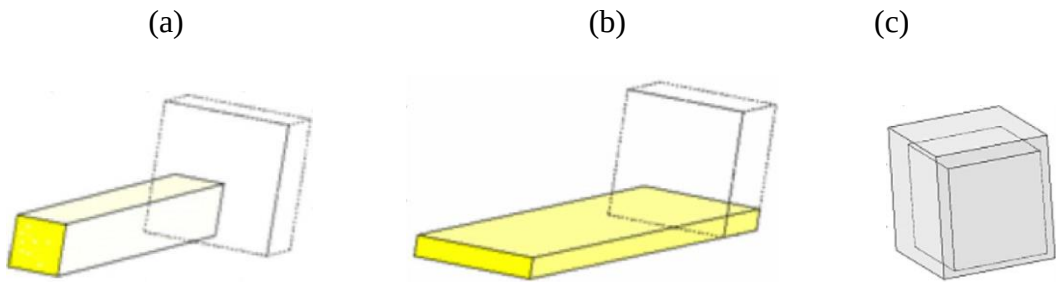

Fig. 3.1 Three Homogeneous Experiment, From[17]

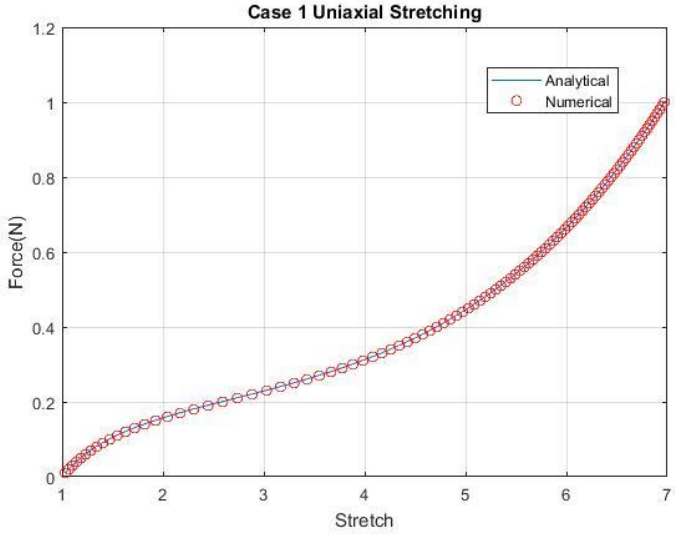

Fig. 3.2 Result under case 1

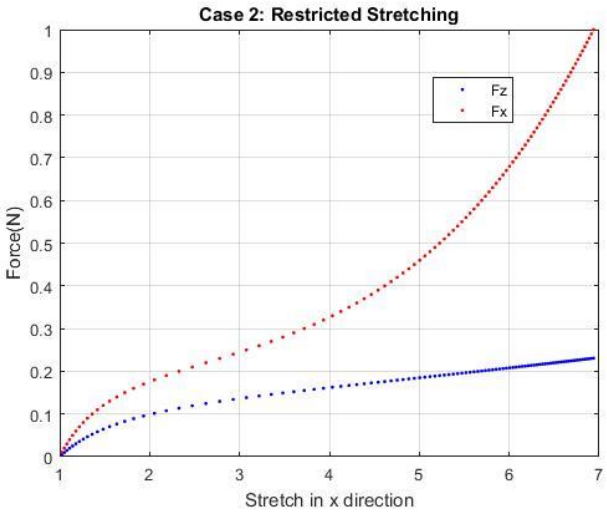

Fig. 3.3 Result under case 2

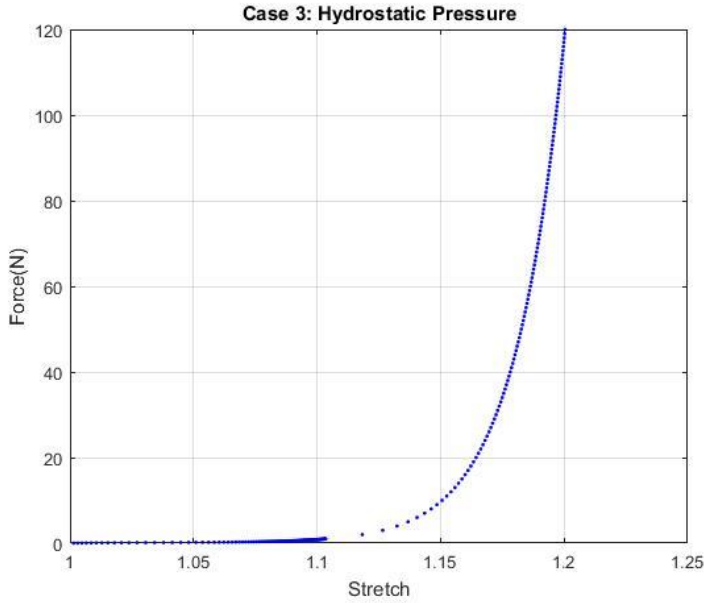

Fig. 3.4 Result under case 3

3.2 Single Element Model of Brain tissue

As is demonstrated in Section 1.2, different sets of brain tissue parameters were derived from the biomaterial testing presented in [11]. In this section, a simulation will be conducted to reproduce

these results. We decided to use the parameters tested from corpus callosum for the whole brain impact presented in Section 3.3.

Ogden material parameters for the corpus callosum were given as:

$$\mu_1 = 0.032kPa, \mu_2 = -0.179kPa,$$
$$\alpha_1 = 11.5, \alpha_2 = -8.1,$$
$$\beta_1 = \beta_2 = 20.$$

These parameters were chosen for the following reasons:

The corpus callosum consists of white matter only [19], so measured material properties are not confounded by a mixture of different materials (e.g. the different ratio of white matter during harvesting of specimen). Also, the absolute value of parameter α is smaller, which will reduce the risk of numerical instabilities for large deformations.

Simulation result for the chosen material parameters are shown in the following Fig. 3.5.

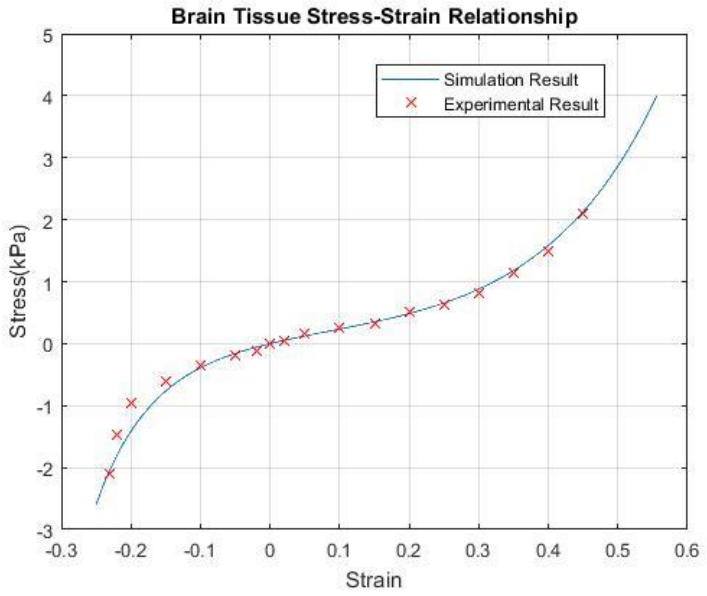

Fig 3.5 Stress-strain relationship for white matter

In Fig. 3.5, the cross means the experimental data visually extracted from a diagram from Fig 4.12 in [11], and the line corresponds to simulation results, demonstrating a good fit at strain range from -0.3 to 0.5.

3.3 Whole Brain Simulation

In this section, a simulation involving whole brain is described.

Based on an anatomical MR image of the human head, a segmentation is performed that defines regions with homogeneous material properties: white matter, grey matter, bone, fluid compartments, meninges, and muscles. Next, a hexahedral mesh is introduced at a resolution of 2.8mm. Each element in this mesh is addressed a material code. A rendering of this mesh is shown below:

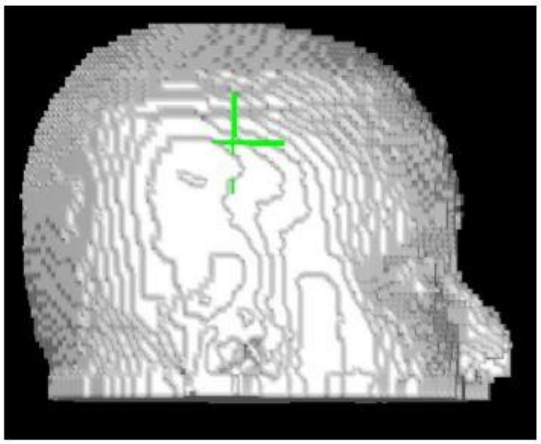

Fig. 3.6 Volumetric mesh, from[20]

The whole brain simulation was conducted under two different kind of model. The first model treats the white matter and gray matter in brain as linear elastic material. The second model treats the white matter and gray matter as nonlinear elastic material (i.e. Ogden material) while the other tissues will still be treated as linear elastic materials.

The linear material properties used in the first simulation are taken from [10]. Detailed properties are listed in the table below:

Tissue	E / [MPa]	ν	Density/[kg/m^3]
Scalp	16.70	0.42	1200
Skull	6500	0.22	1420
White matter	0.12	0.499	1040
Gray matter	0.075	0.499	1040
CSF	0.075	0.49995	1045

Table 3.1 Material parameters used in first simulation

In the second simulation, the nonlinear model with parameters from [11] will be used in both the white matter and gray matter because of the similarity of the experiment result presented in [11]. The other material parameters are the same as in the first simulation:

Tissue		E / [MPa]	ν	Density/[kg/m^3]
Linear	Scalp	16.70	0.42	1200
	Skull	6500	0.22	1420
	CSF	0.075	0.49995	1045
Nonlinear	Brain tissue (white matter and gray matter)	$\mu_1 = 0.032kPa, \mu_2 = -0.179kPa$		
		$\alpha_1 = 11.5, \alpha_2 = -8.1$		
		$\beta_1 = \beta_2 = 20.$		

Table 3.2 Material parameters used in second simulation

Here note that nonlinear parameters shown in Table 3.2 are the parameters of the Ogden model in Eq. (33).

An example impact will be applied at the center of the forehead along the anteroposterior axis and the deformation of the brain tissue will be measured in both situations. The impact is performed as a half-period sinusoidal wave from 0ms to 20ms and has a time step interval of 0.5ms. The peak value of impact force is $1\times10^4 N$. The impact position is position of the cross shown in the following figure:

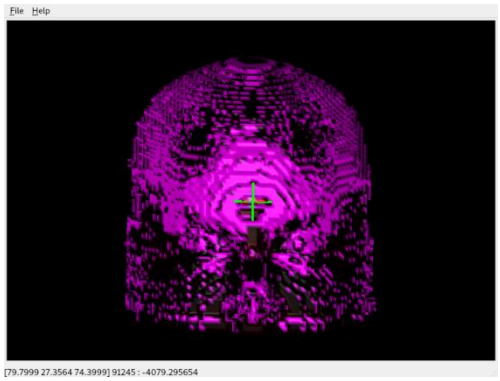

Fig 3.7 Impact position

The test point is chosen in an area of white matter near the impact applying axis, the following figure shows the position of the chosen testing point at the center of the cross:

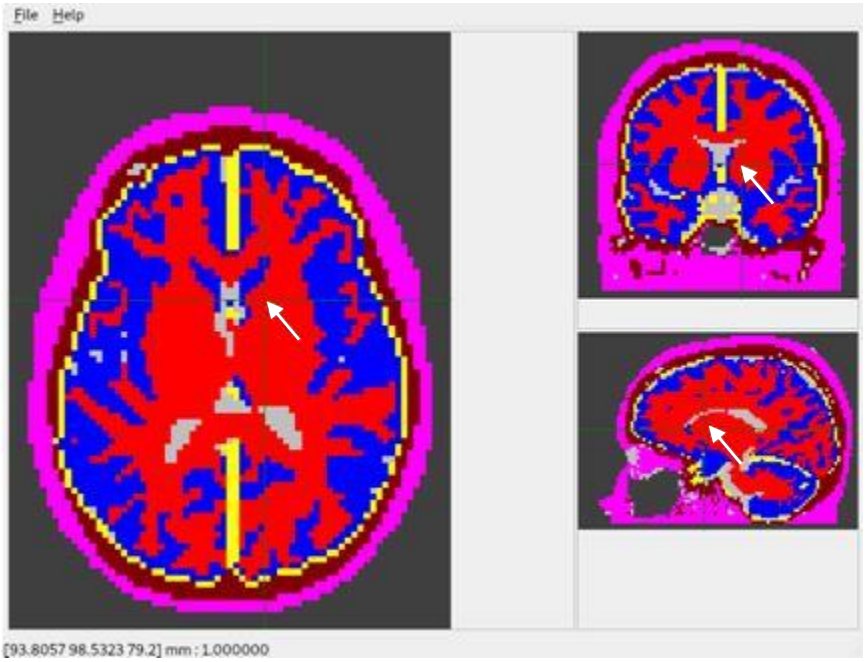

Fig. 3.8 Test point

At the end of every simulation time step, the deformation at the test point is recorded. After completing both simulations, there are two sets of deformation data collected at the test point. The plot of the data is shown in the following figure:

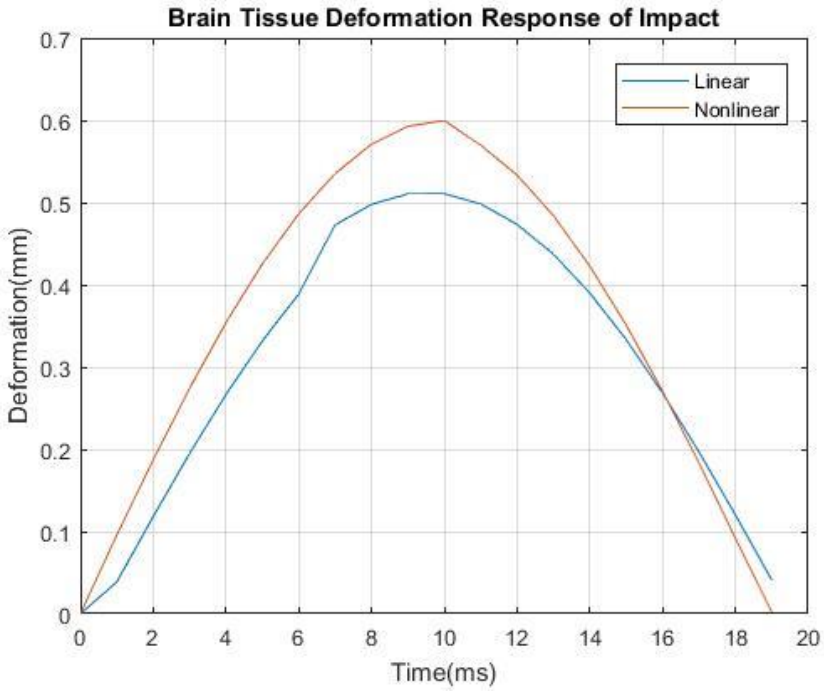

Fig. 3.9 Simulation results

As we can see in Fig. 3.9, the deformation of the brain tissue with nonlinear elasticity is larger than the tissue modeled to have linear elasticity. In fact, the tested deformation in nonlinear model is on average 16.9% larger than the deformation of linear model. It means that the brain will deform more severely to generate enough internal force to balance the influence from the external force.

4 Conclusion and Discussion

The single element simulation result described in Section 3.2 demonstrated a good match with the experiment. This result verifies the Ogden model implemented in the simulator has a good accuracy under uniaxial tension/compression testing.

The whole brain simulation result described in Section 3.3 revealed that the brain tissue modeled by nonlinear properties appears to be more vulnerable and easier to deform with applied external force than the linear model. That means, to balance the same external force, brain tissue with nonlinear properties needs to go through larger deformation to generate sufficient internal force.

In fact, the stress-strain relationship shown in Fig. 3.7 also implies that near a range around the undeformed geometry, with a slight increase in applied force, the brain tissue can easily be deformed from the original shape. However, with the low ability to generate internal force and low capacity of storing elastic potential energy [21], when the force keeps increasing, the brain tissue will stop deforming and start to pass the pressure directly to the tissue nearby.

In this project, the brain tissue is assumed to be isotropic. However, in reality, most of the biomaterials are believed to be anisotropic. The white matter in brain consists of long neuron axons covered in myelin sheath. The mechanical property is definitely different in the direction that is parallel to the axon extending direction or perpendicular to it [7]. The improvement of modeling in anisotropy could be done if reasonable experiment is designed and reliable data of material anisotropy is successfully collected.

The only pattern of the external force used in this project is an impact. However, it is reported that there could be a different frequency response between different elastic models [22]. This frequency response difference could be tested by applying a periodic external force with a specific frequency.

Also, in this project, the possibility of the material breakdown is not considered. In reality, the material can be broken when the external force exceeding some threshold. In terms of brain tissue, this might mean the detachment between neurons or the fracture of the brain tissue, either of them indicates brain damage. This breakdown could be expressed by the sudden change in material stress-strain relationship, which will lead to discontinuity or non-derivability of the strain energy density [23].

The effort on eliminating the limitations discussed above is probably next step of this project. In fact, any effort that makes the result from this simulator closer to the reality as well as decrease time cost of calculation could be the next aim of research in this project.

Reference

[1] Y. Zhang. "A Bio-Medical Model of the Human Head for Impact Simulation", Thesis, UC Irvine, 2015.

[2] J. A. Langlois, W. Rutland-Brown, and K. E. Thomas. "Traumatic brain injury in the United States; emergency department visits, hospitalizations, and deaths." https://www.cdc.gov/traumaticbraininjury/pdf/blue_book.pdf accessed at Dec, 2018.

[3] J. M. Hardman, and A. Manoukian. "Pathology of head trauma." Neuroimaging Clinics of North America 12.2 (2002): 175-87.

[4] M. F.Kraus, T. Susmaras, B. P. Caughlin, C. J. Walker, J. A. Sweeney, and D. M. Little. "White matter integrity and cognition in chronic traumatic brain injury: a diffusion tensor imaging study." Brain 130.10 (2007): 2508-2519.

[5] U. Hartmann, and F. Kruggel. "Transient analysis of the biomechanics of the human head with a high-resolution 3D finite element model." Computer Methods in Biomechanics and Biomedical Engineering 2.1 (1999): 49-64.

[6] E. S. Place, N. D. Evans, and M. M. Stevens. "Complexity in biomaterials for tissue engineering." Nature materials 8.6 (2009): 457.

[7] Y. Feng, R. J. Okamato, R. Namani, G. M. Genin, and P. V. Bayly. "Measurements of mechanical anisotropy in brain tissue and implications for transversely isotropic material models of white matter." Journal of the mechanical behavior of biomedical materials 23 (2013): 117-132.

[8] G. Franceschini, D. Bigoni, P. Regitnig, and G. A. Holzapfel. "Brain tissue deforms similarly to filled elastomers and follows consolidation theory." Journal of the Mechanics and Physics of Solids 54.12 (2006): 2592-2620.

[9] K. De, and J. R. White. Rubber technologist's handbook. Vol. 1. iSmithers Rapra Publishing, Shrewsbury, UK, 2001.

[10] SimBio Consortium. "SimBio: A generic environment for bio-numerical simulation.", NEC Europe Ltd., UK, 2000.

[11] G. Franceschini. "The mechanics of human brain tissue." Modelling, preservation and control of materials and structures, University of Trento, Italy, 2006.

[12] R. W. Ogden. Non-linear elastic deformations. Courier Corporation, Mineola, New York, US, 1997.

[13] N. H. Kim. "Introduction to nonlinear finite element analysis." Springer Science & Business Media, New York, 2015.

[14] D. L. Logan. A first course in the finite element method. Cengage Learning, Stanford, USA, 2011.

[15] Courant, Richard. "Variational methods for the solution of problems of equilibrium and vibrations." Lecture Notes in Pure and Applied Mathematics (1994): 1-1.

[16] K. J. Bathe. Finite element procedures. Prentice Hall, Upper Saddle River, New Jersy, USA, 2006.

[17] F. Peyraut, Z. Q. Feng, Q. C. He, and N. Labed. "Robust numerical analysis of homogeneous and non-homogeneous deformations." Applied Numerical Mathematics 59.7 (2009): 1499-1514.

[18] A. Sprinkart. "A biomechanical finite element model of the human head based on individual medical images using parallel computing", Thesis, University of Bonn, 2010

[19] A. Fitsiori, D. Nguyen, A. Karentzos, J. Delavelle, and M. I. Vargas. "The corpus callosum: white matter or terra incognita." The British journal of radiology 84.997 (2011): 5-18.

[20] Z. Cheng, "Simulation of Traumatic Brain Injury in Children using Finite Element Modeling", Thesis, UC Irvine, 2017.

[21] A. Schettini, and E. K. Walsh. "Brain tissue elastic behavior and experimental brain compression." American Journal of Physiology-Regulatory, Integrative and Comparative Physiology 255.5 (1988): R799-R805.

[22] R. de Rooij, and E. Kuhl. "Constitutive modeling of brain tissue: current perspectives." Applied Mechanics Reviews 68.1 (2016): 010801.

[23] P. M. Duxbury, and P. L. Leath. "Exactly solvable models of material breakdown." Physical Review B 49.18 (1994): 12676.